Nanoscale Advances

ROYAL SOCIETY OF CHEMISTRY

COMMUNICATION

View Article Online
View Journal | View Issue

Check for updates

Cite this: *Nanoscale Adv.*, 2023, **5**, 1631

Received 27th December 2022
Accepted 20th February 2023

DOI: 10.1039/d2na00951j

rsc.li/nanoscale-advances

A bioinspired silica nanocomposite for enhanced multidrug-resistant bacteria treatment and wash-free imaging†

Xiaokun Liu,‡[ab] Zhiying Zhang,‡[a] Nikodem Tomczak,[c] Cong Yang,[a] Chengjun Li, *[a] Rongrong Liu *[a] and Bing Yan [a]

Bacterial infections have posed significant threats to public health due to the emergence of antibiotic resistance. In this work, a novel antibacterial composite nanomaterial based on spiky mesoporous silica spheres loaded with poly(ionic liquid)s and aggregation-induced emission luminogens (AIEgens) was designed for efficient multidrug-resistant (MDR) bacteria treatment and imaging. The nanocomposite exhibited excellent and long-term antibacterial activity towards both Gram-negative and Gram-positive bacteria. Meanwhile, fluorescent AIEgens facilitate real-time bacterial imaging. Our study provides a multifunctional platform and a promising alternative to antibiotics for combating pathogenic MDR bacteria.

Bacterial infections remain one of the most challenging threats to public health today.[1] Although antibiotics have done a great job in preventing the spread of bacteria for several decades, the misuse of antibiotics has made them gradually ineffective.[2,3] Furthermore, the emergence of multidrug-resistant (MDR) bacteria with strong virulence and high lethality has necessitated the development of novel strategies for effective reduction of MDR spread and infections.[4,5] A variety of antimicrobial agents have been explored and widely studied, such as antimicrobial peptides,[6,7] metallic nanoparticles,[8,9] biomacromolecules,[10,11] and so on. However, their widespread applications are limited due to adverse effects, such as leakage of metal ions, cytotoxicity, and hemolysis.[12]

Among the emerging antibacterial materials, ionic liquids have attracted increasing attention in recent years.[13–17] Ionic liquids with cationic charge strongly interact with the negatively charged bacteria. This, in turn, disturbs the structure of bacterial cell membranes, which accelerates membrane damage and bacteria death.[18] Ionic liquids have also shown excellent biocompatibility, which is vital for clinical applications.[17,19] They, therefore, are potential candidates to suppress the spread of multidrug resistance among bacteria in clinical settings. With an increasing number of applications of ionic liquids in pharmaceuticals, adverse effects associated with drug resistance cannot be overlooked.[20–22]

Mesoporous silica nanoparticles (NPs) are noteworthy carriers for delivering antimicrobial agents in the antibacterial field because of their biocompatibility, high loading efficiency, and environment-friendly properties.[23–25] Moreover, it has been reported that the surface roughness of biomaterials is a crucial feature in influencing the material–bacteria interactions.[26,27] Silica spheres with a rough surface like nanopollens derived from natural mimic principles have demonstrated enhanced adhesive properties towards bacteria.[28] Therefore, mesoporous silica nanopollens are promising nanocarriers for delivering and enriching antimicrobials for bacterial treatment to minimize adverse effects.[29,30]

More recently, multifunctional systems integrating monitoring and inhibition of pathogenic bacteria have been used in clinical diagnosis and treatment.[31–34] Aggregation-induced emission (AIE) agents have also been used in developing new luminescent materials for microbial imaging.[35–37] AIE agents emit strong fluorescence when aggregated by restriction of their rotational molecular structure, thus avoiding the unwanted aggregation-caused quenching (ACQ) phenomenon. Therefore, they are ideal luminophores that spontaneously "turn-on" with bacterial concentration when adhered to bacterial surfaces.[35,38,39] Such AIE luminogens can be integrated into multifunctional platforms for bacterial imaging.

A simple and integrated nanocomposite was developed for simultaneous imaging and combating bacteria. Biocompatible AIE agent AFN-I, 3-butyl-1-vinylimidazolium bromide (ILs), and poly(3-butyl-1-vinylimidazolium bromide) (PILs) were used and

[a]*Institute of Environmental Research at Greater Bay Area, Key Laboratory for Water Quality and Conservation of the Pearl River Delta, Ministry of Education, Guangzhou University, Guangzhou, 510006, China. E-mail: liurr@gzhu.edu.cn*

[b]*Southern Marine Science and Engineering Guangdong Laboratory, Zhuhai, 519000, China*

[c]*Institute of Materials Research and Engineering, Agency for Science, Technology and Research (A*STAR), 2 Fusionopolis Way, Innovis #08-03, Singapore 138634, Republic of Singapore*

† Electronic supplementary information (ESI) available. See DOI: https://doi.org/10.1039/d2na00951j

‡ These authors contributed equally to this work.

Open Access Article. Published on 20 February 2023. Downloaded on 8/1/2025 8:17:44 PM. This article is licensed under a Creative Commons Attribution-NonCommercial 3.0 Unported Licence.

© 2023 The Author(s). Published by the Royal Society of Chemistry

Open Access Article. Published on 20 February 2023. Downloaded on 8/1/2025 8:17:44 PM. This article is licensed under a Creative Commons Attribution-NonCommercial 3.0 Unported Licence.

prepared as reported (Fig. S1–S4, ESI†).[38,40] Mesoporous silica hollow nanospheres were employed as vehicles for delivering AFN-I and ILs/PILs. The nanoscale surface roughness of silica spheres would improve their loading and adhesive capabilities, which are beneficial for long-term bacterial treatment. AFN-I with an electron-donor and acceptor structural unit has good dispersibility and a weak fluorescence background in solution. It presented very weak fluorescence on the nanocomposite by retaining its molecular movement. However, the AIE effect could be spontaneously turned on when the nanocomposite was attached and concentrated on the bacterial surface, achieving wash-free imaging of bacteria.

To prove our concept, rough mesoporous silica hollow spheres (R-MSHSs) and smooth silica hollow spheres (S-SHSs) were fabricated with a surfactant-free method at room temperature.[28] Then, PILs and AFN-I were coloaded onto R-MSHSs and S-SHSs to obtain nanocomposites with a rough (R-P-AFN) and smooth (S-P-AFN) surface separately. Transmission electron microscopy (TEM) showed noticeable morphological differences between R-MSHSs and S-SHSs. R-MSHSs had a spiky surface with an average diameter of 190.5 ± 11.42 nm and a hydrodynamic diameter of 275 ± 2.48 nm (Fig. 1A and Table S2†). The mean particle diameter of S-SHSs was 221 ± 12.21 nm with a hydrodynamic diameter of 229 ± 1.64 nm (Fig. 1B and Table S2†). After adsorbing PILs and AFN-I on the nanosphere surface, different degrees of diameter increase were observed. The diameter of R-P-AFN was increased by 51.4 nm to 241.4 ± 21.04 nm, with a hydrodynamic diameter of 285.7 ± 1.42 nm. Similarly, there was also a slight increase in S-P-AFN diameter (231.6 ± 14.4 nm) as well as the hydrodynamic diameter (255.7 ± 2.57 nm) (Fig. S5 and Table S2†). The surface morphologies of R-P-AFN and S-P-AFN were also determined from SEM images (Fig. 1C and D). Additionally, the porosities of R-MSHSs and S-SHSs were characterized using nitrogen sorption analysis. The Brunauer–Emmett–Teller (BET) surface area and the total pore volume of R-MSHSs are 118.7 m^2 g^{-1} and 0.32 cm^3 g^{-1}, respectively. The corresponding pore size distribution curve shows that R-MSHSs possess a pore diameter of 9.1 nm (Fig. S6†). Compared with R-MSHSs, S-SHSs have a low surface area of 66.9 m^2 g^{-1} with no obvious identified pores.

Antibacterial experiments using ILs and PILs were performed against *Escherichia coli* (*E. coli*), *Staphylococcus aureus* (*S. aureus*), MDR Enteropathogenic *Escherichia coli* (EPEC), and Methicillin-resistant *S. aureus* (MRSA). The bactericidal properties of both agents were found to be more effective against the Gram-positive bacteria (*S. aureus* and MRSA) than the corresponding Gram-negative bacteria (*E. coli* and EPEC) (Fig. 2). Moreover, PILs exhibited enhanced antibacterial efficacy by two to three orders of magnitude than ILs against bacteria and the corresponding MIC values were determined (Table S3†). Gram-positive bacteria lack an outer cell membrane and have a thick peptidoglycan layer that favors the interactions with ionic liquids and become disrupted, leading to the internal cytoplast leakage and cell death.[29] Compared with common strains, MDR bacteria showed higher sensitivity to ionic liquids, which may be caused by modification of electrokinetic potential, change of membrane permeability, surface functional proteins, and their steric interactions between ionic liquids and bacterial strains.[5,41–44]

PILs and AFN-I were further co-adsorbed on the nanospheres. As shown in Fig. 3A, the surface potential of the nanospheres exhibited distinct changes. As expected, due to the loading of positively charged PILs and AFN-I, the zeta potential of R-P-AFN and S–P-AFN was significantly changed from −24.4 mV and −33.3 mV to +58.8 mV and +50.8 mV, respectively. The positive surface charge of the nanocomposites is favorable for bacterial adhesion through electrostatic interactions. The loading capacities of the two nanospheres were also compared for the antibacterial agents. As shown in Fig. 3B, R-MSHSs exhibited a higher loading capacity for both ILs (2.90 mg g^{-1}) and PILs (88.60 mg g^{-1}). By contrast, due to the limited external surface, the loading capacity of S-SHSs for ILs and PILs was 1.02 mg g^{-1} and 60.28 mg g^{-1}, respectively. These results align well with their morphology difference after loading, suggesting that the nanospheres with a rough surface have greater loading capability.

The antibacterial effects of nanocomposites loaded with ILs and PILs toward bacteria were investigated. Specifically, R-MSHSs and S-SHSs were loaded with IL and PILs, respectively, resulting in four different types of nanocomposites, including R-MSHSs loaded with ILs (R-ILs) and PILs (R-PILs), and S-SHSs loaded with ILs (S-ILs) and PILs (S-PILs). Bacteria (1×10^7 CFU mL^{-1}) were incubated with the obtained nanocomposites for

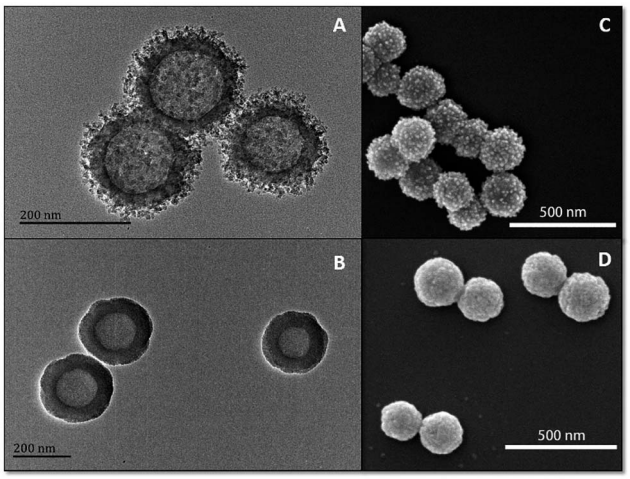

Fig. 1 TEM images of R-MSHSs (A) and S-SHSs (B). SEM images of R-P-AFN (C) and S-P-AFN (D).

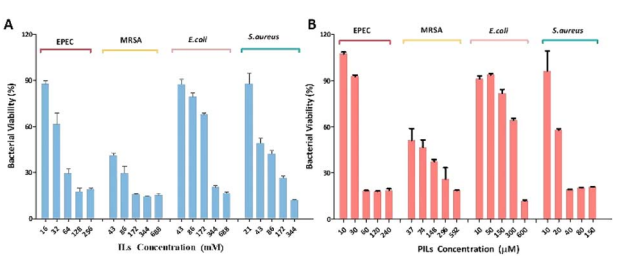

Fig. 2 Dose-dependent antibacterial activities of (A) ILs and (B) PILs toward *E. coli*, *S. aureus*, EPEC, and MRSA after 24 h.

© 2023 The Author(s). Published by the Royal Society of Chemistry

Open Access Article. Published on 20 February 2023. Downloaded on 8/1/2025 8:17:44 PM.
This article is licensed under a Creative Commons Attribution-NonCommercial 3.0 Unported Licence.

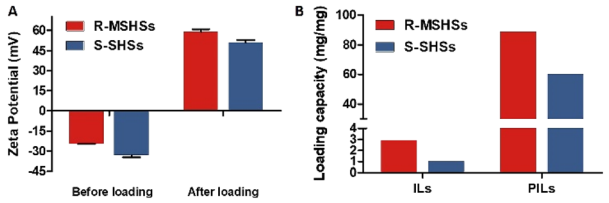

Fig. 3 (A) Zeta potential changes of nanocomposites before and after AFN-I and PIL loading. (B) IL and PIL loading capacity of R-MSHSs and S-SHSs.

24 h. The antibacterial activity of the nanocomposites was evaluated by the colony formation unit (CFU) inhibition assay.

As shown in Fig. 4, after loading with ILs or PILs, the nanocomposites showed distinctly different antibacterial effects. For the same type of antimicrobial agent, nanocomposites with rough surfaces exhibited higher antibacterial activity than those with smooth surfaces. R-PILs almost completely inhibited (>98%) all the strains. These results are attributed to the improved drug loading capacity and enhanced bacterial adhesion performance of rough silica nanospheres, suggesting the advantage of R-MSHSs as a carrier of antimicrobial agents. In addition, the toxicity of core nanospheres on bacteria growth was assessed by a dose-dependent assay. Both bare silica nanospheres exhibited less than 20% bacterial inhibition at concentrations up to 0.5 mg mL^{-1}, which indicates that the core nanospheres have relatively low toxicity to bacteria (Fig. S7†).

AFN-I, a probe molecule with AIE properties, was adsorbed onto the nanospheres to evaluate wash-free bacterial imaging. The fluorescence intensity changes of AFN-I with different bacterial concentrations were determined (Fig. S8†). No fluorescence of AFN-I was observed in water due to its excellent solubility. However, with the increased concentration of bacteria, significant emission enhancement at 560 nm was observed. The positively charged AFN-I interacted with the bacterial surface, leading to the aggregation and enhanced emission of AFN-I. We further stained *E. coli* with R-P-AFN. The pure R-P-AFN solution had a weak emission under 365 nm irradiation. After incubation with bacteria, R-P-AFN efficiently adhered to the bacteria, restricting the intramolecular motion of AFN-I and contributing to distinct fluorescence enhancement by about seven fold at 560 nm (Fig. S9 and S10†). As a result, strong orange fluorescence under 365 nm irradiation was observed.

To demonstrate the interaction between R-P-AFN and bacteria, *E. coli* was simultaneously stained with SYTO and AFN-I/R-P-AFN and then imaged using confocal laser scanning microscopy (CLSM). SYTO stains the bacteria in green color, while the false red emission from the bacteria presents the fluorescence of AFN-I (Fig. 5A–F). As shown in Fig. 5E, the bacteria were observed to form aggregates with an irregular morphology after the treatment of R-P-AFN. More insights into the nanocomposite–bacteria interactions were obtained from SEM characterization. The rod-like *E. coli* surfaces after treatment with R-P-AFN had a roughened and flaked appearance compared to the intact smooth cells (Fig. 5G and H). The nanocomposites were observed to adhere to the cell surface and the distortion of cellular morphology was clearly visible due to the PIL effects. Overall, the above results demonstrated the antibacterial potential of R-P-AFN towards bacteria and its simultaneous wash-free imaging capability.

In conclusion, we have successfully developed a multifunctional nanocomposite R-P-AFN for bacterial treatment and wash-free bacterial imaging. This novel nanocomposite is facilely prepared. In the presence of AFN-I, R-P-AFN is equipped with AIE properties. The mesoporous silica hollow nanospheres with a rough surface can serve as the carriers for PILs and enable bacterial long-term anchoring due to their spiky

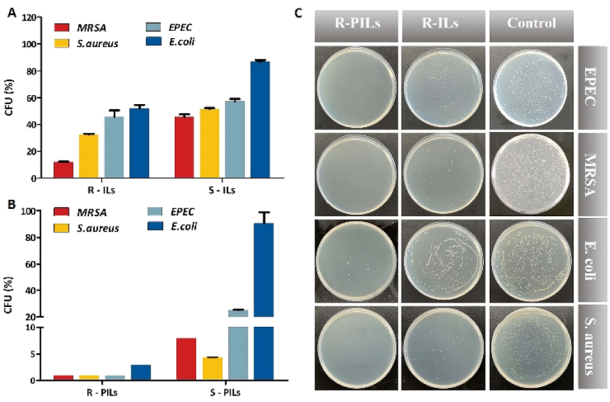

Fig. 4 Antibacterial activity of R-MSHSs loaded with ILs (R-ILs) and PILs (R-PILs), and S-SHSs loaded with ILs (S-ILs) and PILs (S-PILs). Inhibition experiment with (A) R-ILs, S-ILs, (B) R-PILs, and S-PILs against *E. coli*, *S. aureus*, EPEC, and MRSA. (C) Images of agar plates for *E. coli*, *S. aureus*, EPEC, and MRSA with nanocomposites for 24 h treatment.

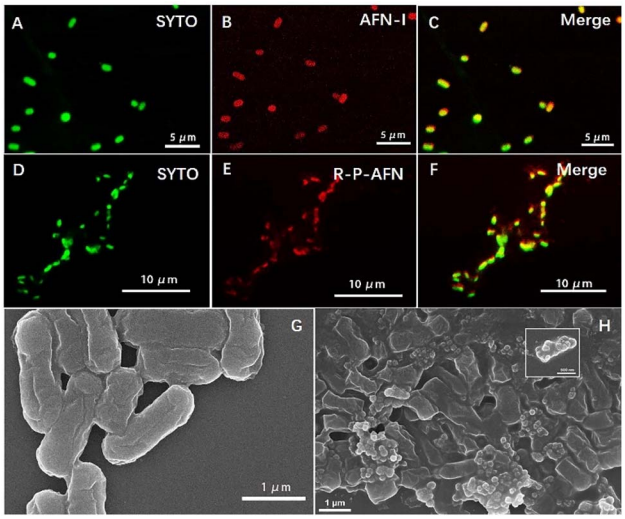

Fig. 5 CLSM images of (A and D) *E. coli* cells labeled with SYTO (green), (B) *E. coli* cells treated with 15 μM AFN-I for 30 min with a false red emission of the bacterial membranes, (E) *E. coli* cells treated with nanocomposites (R-P-AFN) with false red emission of the bacterial membranes, and (C and F) overlay images. SEM images of (G) blank *E. coli* and (H) *E. coli* treated with R-P-AFN. (*E. coli*, 1×10^7 CFU mL^{-1}; AFN-I $\lambda_{ex} = 405$ nm; SYTO $\lambda_{ex} = 500$ nm).

© 2023 The Author(s). Published by the Royal Society of Chemistry

Open Access Article. Published on 20 February 2023. Downloaded on 8/1/2025 8:17:44 PM. This article is licensed under a Creative Commons Attribution-NonCommercial 3.0 Unported Licence.

topological features. Benefitting from the enhanced membrane interactions with PILs, R-P-AFN has an excellent antibacterial ability to combat Gram-positive and Gram-negative bacteria. More importantly, R-P-AFN can kill MDR bacteria that pose significant challenges in healthcare. Our study provides a novel strategy for real-time imaging and the prevention of MDR bacterial infection.

Author contributions

X. Liu & Z. Zhang: conceptualization, methodology, investigation, formal analysis, data curation, writing – original draft. N. Tomczak: investigation, validation, writing – review & editing. C. Yang: investigation, formal analysis. C. Li: resources, supervision, validation, writing – review & editing. R. Liu: conceptualization, resources, supervision, validation, writing – review & editing. B. Yan: resources, supervision, writing – review & editing.

Conflicts of interest

There are no conflicts to declare.

Acknowledgements

This work was financially supported by the Natural Science Foundation of Guangdong Province (2022A1515010366), the National Natural Science Foundation of China (222006025), the Guangzhou Municipal Science and Technology Project (202102010437), and the Introduced Innovative R&D team project under the "The Pearl River Talent Recruitment Program" of Guangdong Province (2019ZT08L387).

Notes and references

1 E. D. Brown and G. D. Wright, *Nature*, 2016, **529**, 336–343.
2 Y. Wang, Y. Yang, Y. Shi, H. Song and C. Yu, *Adv. Mater.*, 2020, **32**, e1904106.
3 R. Liu, R. Liew, J. Zhou and B. Xing, *Angew. Chem., Int. Ed.*, 2007, **46**, 8799–8803.
4 L. Dijkshoorn, A. Nemec and H. Seifert, *Nat. Rev. Microbiol.*, 2007, **5**, 939–951.
5 C. Mao, W. Jin, Y. Xiang, Y. Zhu, J. Wu, X. Liu, S. Wu, Y. Zheng, K. M. C. Cheung and K. W. K. Yeung, *Adv. Funct. Mater.*, 2022, **32**, 2202887.
6 Z. Ma, D. Wei, P. Yan, X. Zhu, A. Shan and Z. Bi, *Biomaterials*, 2015, **52**, 517–530.
7 L. Nystrom, N. Al-Rammahi, S. Malekkhaiat Haffner, A. A. Stromstedt, K. L. Browning and M. Malmsten, *Biomacromolecules*, 2018, **19**, 4691–4702.
8 Z. Fan, B. Liu, J. Wang, S. Zhang, Q. Lin, P. Gong, L. Ma and S. Yang, *Adv. Funct. Mater.*, 2014, **24**, 3933–3943.
9 W.-Y. Chen, H.-Y. Chang, J.-K. Lu, Y.-C. Huang, S. G. Harroun, Y.-T. Tseng, Y.-J. Li, C.-C. Huang and H.-T. Chang, *Adv. Funct. Mater.*, 2015, **25**, 7189–7199.
10 C. D. Fjell, J. A. Hiss, R. E. Hancock and G. Schneider, *Nat. Rev. Drug Discovery*, 2011, **11**, 37–51.
11 R. T. Cleophas, J. Sjollema, H. J. Busscher, J. A. Kruijtzer and R. M. Liskamp, *Biomacromolecules*, 2014, **15**, 3390–3395.
12 Y. Zhang, P. Sun, L. Zhang, Z. Wang, F. Wang, K. Dong, Z. Liu, J. Ren and X. Qu, *Adv. Funct. Mater.*, 2019, **29**, 1808594.
13 Z. Q. Zheng, Q. M. Xu, J. N. Guo, J. Qin, H. L. Mao, B. Wang and F. Yan, *ACS Appl. Mater. Interfaces*, 2016, **8**, 12684–12692.
14 W. Zheng, W. Huang, Z. Song, Z. Tang and W. Sun, *Phys. Chem. Chem. Phys.*, 2020, **22**, 15573–15581.
15 J. C. Stockert, R. W. Horobin, L. L. Colombo and A. Blazquez-Castro, *Acta Histochem.*, 2018, **120**, 159–167.
16 W. Zhang, Y. Huang, Y. Chen, E. Zhao, Y. Hong, S. Chen, J. W. Y. Lam, Y. Chen, J. Hou and B. Z. Tang, *ACS Appl. Mater. Interfaces*, 2019, **11**, 10567–10577.
17 S. N. Riduan and Y. Zhang, *Chem. Soc. Rev.*, 2013, **42**, 9055–9070.
18 D. Bains, G. Singh, J. Bhinder, P. K. Agnihotri and N. Singh, *ACS Appl. Bio Mater.*, 2020, **3**, 2092–2103.
19 A. Garcia-Sampedro, A. Tabero, I. Mahamed and P. Acedo, *J. Porphyrins Phthalocyanines*, 2019, **23**, 11–27.
20 K. S. Egorova, E. G. Gordeev and V. P. Ananikov, *Chem. Rev.*, 2017, **117**, 7132–7189.
21 Y. Luo, Q. Wang, Q. Lu, Q. Mu and D. Mao, *Environ. Sci. Technol. Lett.*, 2015, **2**, 165.
22 P. C. Alves, D. O. Hartmann, O. Núñez, I. Martins, T. L. Gomes, H. Garcia, M. T. Galceran, R. Hampson, J. D. Becker and C. Silva Pereira, *BMC Genomics*, 2016, **17**, 284.
23 C. Marambio-Jones and E. M. V. Hoek, *J. Nanopart. Res.*, 2010, **12**, 1531–1551.
24 Q. Li, Y. Wu, H. Lu, X. Wu, S. Chen, N. Song, Y. W. Yang and H. Gao, *ACS Appl. Mater. Interfaces*, 2017, **9**, 10180–10189.
25 M. J. Hajipour, K. M. Fromm, A. A. Ashkarran, D. Jimenez de Aberasturi, I. R. de Larramendi, T. Rojo, V. Serpooshan, W. J. Parak and M. Mahmoudi, *Trends Biotechnol.*, 2012, **30**, 499–511.
26 V. K. Truong, R. Lapovok, Y. S. Estrin, S. Rundell, J. Y. Wang, C. J. Fluke, R. J. Crawford and E. P. Ivanova, *Biomaterials*, 2010, **31**, 3674–3683.
27 M. Chen, Q. Yu and H. Sun, *Int. J. Mol. Sci.*, 2013, **14**, 18488–18501.
28 H. Song, Y. Ahmad Nor, M. Yu, Y. Yang, J. Zhang, H. Zhang, C. Xu, N. Mitter and C. Yu, *J. Am. Chem. Soc.*, 2016, **138**, 6455–6462.
29 C. Zhou, F. Wang, H. Chen, M. Li, F. Qiao, Z. Liu, Y. Hou, C. Wu, Y. Fan, L. Liu, S. Wang and Y. Wang, *ACS Appl. Mater. Interfaces*, 2016, **8**, 4242–4249.
30 Y. Xi, T. Song, S. Tang, N. Wang and J. Du, *Biomacromolecules*, 2016, **17**, 3922–3930.
31 E. Zhao, Y. Chen, H. Wang, S. Chen, J. W. Lam, C. W. Leung, Y. Hong and B. Z. Tang, *ACS Appl. Mater. Interfaces*, 2015, **7**, 7180–7188.
32 N. Zehra, D. Dutta, A. H. Malik, S. S. Ghosh and P. K. Iyer, *ACS Appl. Mater. Interfaces*, 2018, **10**, 27603–27611.
33 M. Wang, J. Shi, H. Mao, Z. Sun, S. Guo, J. Guo and F. Yan, *Biomacromolecules*, 2019, **20**, 3161–3170.

© 2023 The Author(s). Published by the Royal Society of Chemistry

Open Access Article. Published on 20 February 2023. Downloaded on 8/1/2025 8:17:44 PM.
This article is licensed under a Creative Commons Attribution-NonCommercial 3.0 Unported Licence.

34 L. Zhao, Y. Chen, J. Yuan, M. Chen, H. Zhang and X. Li, *ACS Appl. Mater. Interfaces*, 2015, **7**, 5177–5186.
35 J. Mei, Y. Huang and H. Tian, *ACS Appl. Mater. Interfaces*, 2018, **10**, 12217–12261.
36 E. Zhao, Y. Hong, S. Chen, C. W. Leung, C. Y. Chan, R. T. Kwok, J. W. Lam and B. Z. Tang, *Adv. Healthcare Mater.*, 2014, **3**, 88–96.
37 Y. Hong, J. W. Y. Lam and B. Z. Tang, *Chem. Soc. Rev.*, 2011, **40**, 5361–5388.
38 L. Huang, S. Li, X. Ling, J. Zhang, A. Qin, J. Zhuang, M. Gao and B. Z. Tang, *Chem. Commun.*, 2019, **55**, 7458–7461.
39 M. Gao, H. Su, Y. Lin, X. Ling, S. Li, A. Qin and B. Z. Tang, *Chem. Sci.*, 2017, **8**, 1763–1768.
40 Z. Zheng, Q. Xu, J. Guo, J. Qin, H. Mao, B. Wang and F. Yan, *ACS Appl. Mater. Interfaces*, 2016, **8**, 12684–12692.
41 A. Borkowski, M. Syczewski and A. Czarnecka-Skwarek, *RSC Adv.*, 2019, **9**, 28724–28734.
42 K. N. Ibsen, H. Ma, A. Banerjee, E. E. L. Tanner, S. Nangia and S. Mitragotri, *ACS Biomater. Sci. Eng.*, 2018, **4**, 2370–2379.
43 M. Baym, L. K. Stone and R. Kishony, *Science*, 2016, **351**, aad3292.
44 M. Baym, T. D. Lieberman, E. D. Kelsic, R. Chait, R. Gross, I. Yelin and R. Kishony, *Science*, 2016, **353**, 1147–1151.

© 2023 The Author(s). Published by the Royal Society of Chemistry